Recent Developments in Modelling Acoustic Reflection Loss at the Rough Ocean Surface

Adrian D. Jones (1), Alec J. Duncan (2), David W. Bartel (1), Alex Zinoviev (1) and Amos Maggi (2)

(1) Defence Science and Technology Organisation, P.O. Box 1500, Edinburgh, SA 5111, Australia
(2) Centre for Marine Science & Technology, Curtin University of Technology, GPO Box U1987, Perth WA 6845, Australia

ABSTRACT

The transmission of sonar signals in a surface ducted environment, or in a shallow ocean, is affected by reflection losses at the ocean surface, when wind action or swell causes the surface to be roughened. Under these circumstances, the amplitude of the specular reflection of sound at the ocean surface is reduced by a number of complex phenomena, including: the sea surface shape; acoustic shadowing of parts of the surface to sound incident at small angles; diffraction of sound into the shadow zones; and bubble formation from white-caps. Recent work has shown that the inclusion of these effects within a ray model of transmission is a formidable prospect, as ray theory cannot describe all the phenomena explicitly, and the inclusion of acoustic wave effects in combination with a ray model is required. This paper addresses several of the complexities, in the search for a comprehensive solution to this modelling issue. In particular, the appropriateness of the Small-Slope Approximation roughness model used by Williams et al. (JASA, 116, Oct. 2004) is investigated, using a Parabolic Equation (PE) model. Also, the refraction near the ocean surface caused by wind-induced bubbles (e.g. Ainslie, JASA, 118, Dec. 2005) is investigated using the PE model. Lastly, the surface loss values obtained for received coherent sound pressure are compared with those relevant to received root-mean-square sound pressure. The paper speculates on the prospects for the future development of a surface loss model that includes all relevant effects.

INTRODUCTION

There has been much work relating to surface acoustic reflection loss, however the subject persists as one for which there is no recognised complete solution. Much of the earlier work (e.g. Marsh et al., 1961), plus more recent work (e.g. Williams et al., 2004), was focussed on descriptions of loss due to the roughness of the surface. The added complication of shadowing of the surface (e.g. Wagner, 1967) had been expected to be relevant, due to the small incidence angles predicted at the surface for ducted transmission (e.g. the angle of a limiting ray as shown in fig. 6.5, Urick 1983) and the fact that sea surface slopes would exceed these angles for all but low sea states. More recently, Ainslie (2005, 2010) showed the transformative effects of incorporating the result of wind-induced bubbles, both refractive effects due to the air fraction distribution near the surface, and the absorption and scattering effects. In earlier work by the present authors (Jones et al., 2010, 2011), the refractive effects due to bubbles were also studied briefly. Ray-theory modelling showed that this refraction caused surface-ducted sound to be incident at the surface at a very small span of angles, so that a single angle of surface incidence could be assumed for each wind speed. However, it was also shown (Jones et al. 2011) that Snell's Law refraction could not necessarily be assumed within the bubbly region, so the adoption of a simplified modelling solution was by no means straightforward.

This paper commences with a brief review of the models of surface roughness loss under consideration. Particular attention is given to the Kirchhoff model and its relativity to the small-slope model used by Williams et al. (2004). Next, the Snell's Law-based inclusion of the refractive effects due to wind-induced bubbles in ray-based modelling is reviewed. The need to consider full acoustic wave effects within the bubbly region, that is, non-adherence to Snell's Law, is then indicated. The relevant effects are demonstrated using stochastic, numerical techniques based on the application of a Parabolic Equation (PE) model. Lastly, a theoretical analysis (Brekhovskikh, 1960) is used to derive a correction to the Snell's law refraction, and the utility of this correction is demonstrated by means of stochastic simulations of the acoustic field for a particular surface duct scenario. The use of this correction may be anticipated to be an inclusion within a practical modelling approach. To maintain comparison with the work of Williams et al. (2004), the acoustic frequencies selected for study are 3200 Hz and 6000 Hz.

SURFACE ROUGHNESS LOSS MODELS

The models considered in this study describe the coherent surface reflection coefficient at the specular angle, due to the roughness of a sea surface caused by wind action. These include: (i) the small-slope approximation (SSA) model as used by Williams et al. (2004), for which the sea surface is assumed to have a Pierson-Moskowitz (PM) surface wave spectrum; (ii) the model presented by Ainslie (2005, 2010) which was based on the perturbation method of Brekhovskikh and Lysanov and (iii) the Kirchhoff model for a sea surface with a Gaussian distribution of surface heights (KA) (e.g. Lurton, 2002, section A.3.3). Ainslie produced a model for each of PM and Neumann-Pierson surface wave spectra – the former is considered here.

Kirchhoff Model

The Kirchhoff, or tangent plane, approximation is based on the assumption that the reflection at every location on the surface occurs as if the surface was locally flat. As stated by Ogilvy (1987) section 6, for example, the requirement for flatness implies that the radius of curvature of the surface ρ ,

in metres, must be sufficiently large that $k\rho\sin^3\beta >> 1$, where β is the acoustic grazing angle with the mean surface plane, radians; k is acoustic wavenumber $2\pi f/c_w$; f is cyclic frequency, Hz; c_w is speed of sound in seawater, m/s. The Kirchhoff approximation is thus expected to fail for appropriately small grazing angles. A further assumption usually applied to closed-form evaluations of surface loss is that a direction normal to the surface is assumed approximately the same as a normal to the mean plane (e.g. Ogilvy (1987) section 6.2). This will be accurate for small slopes.

The determination of reflection loss thus proceeds by the assumption of a phase coherent addition of the specular reflection contributions from sections of surface which are displaced vertically by differing amounts. In application of the technique, the distribution of surface heights is the key input, whilst spatial correlation and movement of surface features are ignored. The model assumes (i) an incident plane wave of infinite extent, (ii) a reflected plane wave of infinite extent which is sampled at large distance from the mean plane of reflection, (iii) a plane scattering surface of infinite extent, with local surface displacements, (iv) continuous insonification of the surface. There is no net energy loss, and a reduction in intensity in the specular direction is balanced by energy scattered to other directions. As the extent of the reflecting sea surface is assumed infinite, the loss is identical for all possible realisations of the sea surface shape that match the prescribed distribution of heights.

The Kirchhoff roughness model for a sea surface with a Gaussian distribution of surface heights (KA) is usually expressed in terms of rms height h_σ of the sea surface. The coherent reflection loss (*RL*) for a single surface reflection, in terms of the Rayleigh parameter $\Gamma = (4\pi f h_\sigma \sin\beta)/c_w$, is

$$RL = -20\log_{10}\left(e^{-0.5\Gamma^2}\right) \text{ dB per bounce.} \qquad (1)$$

By taking the well-known relation $h_\sigma \approx 5.3\times10^{-3}(w_{19.5})^2$ for a PM surface wave spectrum (e.g. section 13.1 of Medwin and Clay, 1998), where $w_{19.5}$ is wind speed measured 19.5 m above sea level, *RL* for the KA model becomes

$$RL \approx 0.019\left[f(w_{19.5})^2\sin\beta/c_w\right]^2 \text{ dB.} \qquad (2)$$

Ainslie Model

Following the perturbation method used by Brekhovskikh and Lysanov (2003), section 9.6, Ainslie (2005) derived expressions for the coherent sound pressure reflection coefficient for sea surfaces with a PM wave spectrum. Ainslie's expression is equivalent to a reflection loss per bounce as

$$RL \approx 2.60\times10^{-7} f^{3/2}(w_{19.5})^3\sin\beta \text{ dB.} \qquad (3)$$

Small-slope Approximation Model

The algorithm for the small-slope approximation (SSA) model used by Williams et al. (Williams et al., 2004, equation 14) has been implemented by the Defence Science and Technology Organisation (DSTO). Although not shown here, in this work it has been established that the SSA function for small grazing angles $\beta \to 0$ is $RL \approx 3.12\,\alpha(k/K_L)^{3/2}\beta$, where $K_L = g\sqrt{B}/(w_{19.5})^2$ is a surface wave-number expressing a correlation length, $\alpha = 0.0081$ and $B = 0.74$ are parameters of the PM surface wave spectrum, and $g = 9.81$ m/s^2 is gravitational acceleration. The reflection loss per bounce for the SSA model is thus a linear function of grazing angle for small angles, and in terms of wind speed $w_{19.5}$ and acoustic frequency f is

$$RL \approx 2.79\times10^{-7} f^{3/2}(w_{19.5})^3\beta \text{ dB.} \qquad (4)$$

For small $\beta \approx \sin\beta$, the Ainslie PM model and the linear approximation to SSA are identical, apart from a 7% difference in the constant. Figure 1 shows a typical comparison of the key models (KA, SSA, linear approximation to SSA) for an example for which Γ has a maximum value of about 1.3.

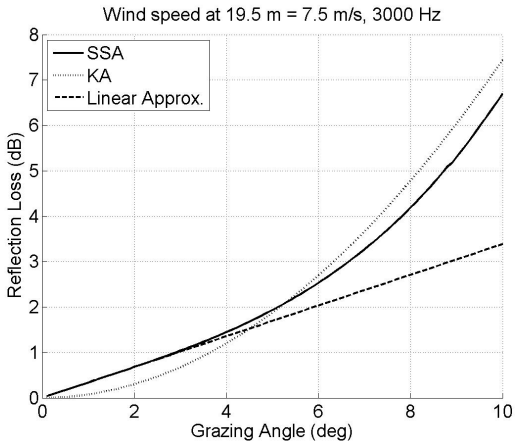

Figure 1. Reflection Loss per bounce, 7.5 m/s wind speed $w_{19.5}$, 3000 Hz

At low grazing angles, the linear approximation is close to the full SSA result, but at steeper angles the loss described by the full model rises more steeply. Earlier work (Jones et al., 2010, and Figure 4 below) achieved a measure of validation of the SSA model in stochastic simulations mentioned later in this paper. Here, the loss values obtained via stochastic simulation for grazing angles from 1º to 7º for 3200 Hz and wind speeds $w_{19.5}$ 5 m/s and 10 m/s were very close to those predicted by the SSA model at all the grazing angles considered, with values of Rayleigh parameter Γ as much as 1.7 for the steepest angle and higher wind speed. The authors intend to extend this validation by similar means but at present have accepted the SSA model as accurate.

From numeric calculation, it has been found that the loss from the SSA model tends toward that from the KA model when the result from Equation (2) exceeds that from Equation (4). A reasonable approximation to the SSA model is then to take the maximum value of the linear approximation and the KA model. This has been found suitable for frequencies 1 kHz to 7 kHz for wind speeds from 3 m/s to 12.5 m/s. At frequencies 8 kHz to 10 kHz the approximation is valid for wind speeds 3 m/s to 10 m/s, and at 500 Hz for wind speeds 5 m/s to 15 m/s. Additional examples are included as Figure 2 (5 m/s wind speed, 6000 Hz), and Figure 3 (7.5 m/s wind speed, 6000 Hz) for which this proposed simplification of the full SSA model appears to be appropriate.

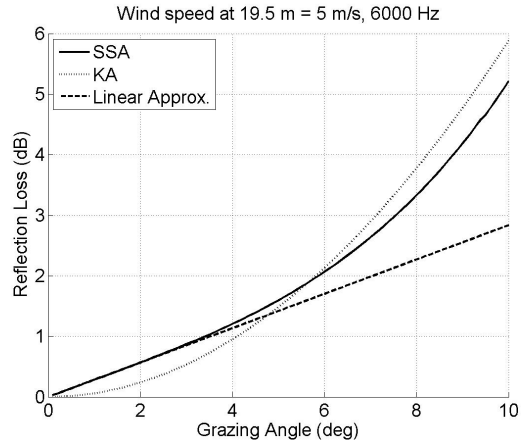

Figure 2. Reflection Loss per bounce, 5 m/s wind speed $w_{19.5}$, 6000 Hz

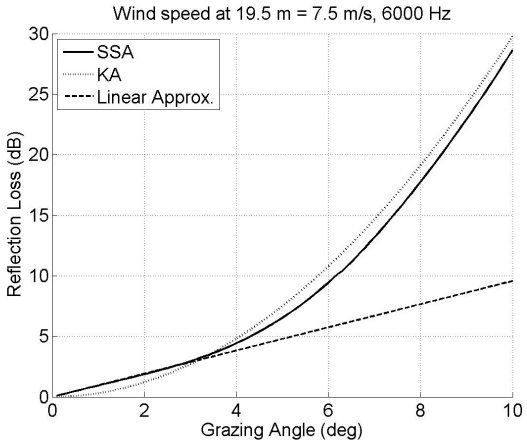

Figure 3. Reflection Loss per bounce, 7.5 m/s wind speed $w_{19.5}$, 6000 Hz

STOCHASTIC MODELLING OF REFLECTION LOSS

In earlier work (Jones et al., 2010, 2011), values of coherent surface reflection loss per bounce were determined via numerical simulations of transmission in an ocean with sea surface boundary shapes based on samples of a stochastic process that satisfied the PM wave spectrum. The PE transmission code RAMSurf (NRL n.d.) was used, and thus all physical effects including acoustic shadowing of segments of the sea surface and diffraction of sound into shadowed zones were implicitly included. Each surface ducted scenario was devised so that the incidence angles at the surface were confined to a small span around a preferred nominal value, with each scenario thus providing data for that angle. For each scenario, the field was computed, first for a smooth surface, then with the surface described as rough, with, typically, 40 random replications of the rough sea surface, with the coherent field determined for each. The stochastic process that was used to generate each surface shape ensured that vertical displacement and horizontal spatial correlation was appropriate to the PM wave spectrum. The total loss of coherent transmission, in dB, was determined by referencing the amplitude of the mean of the coherent pressure fields obtained for the rough surface to the amplitude of the field obtained with the smooth surface. Loss per bounce was then determined. This modelling described a one-dimensional sea surface with transmission for cylindrical symmetry.

Values of reflection loss per bounce from this stochastic modelling were compared with the SSA model for wind speeds 5 m/s and 10 m/s at 3.2 kHz. Figure 4 shows the latter set of data, with the loss values from stochastic modelling shown by rectangles for which the height represents ±2 standard deviations of the mean loss, and the width represents the span of angles over which the trapped beam of rays from the source impinged on the ocean surface (Jones et al. 2010). As Figure 4 shows, this work was supportive of the SSA model. There was no evidence of effects due to surface shadowing, for which loss values in excess of the SSA model would have been expected. Presumably, at 3200 Hz the shadow zones were fully insonified by diffraction.

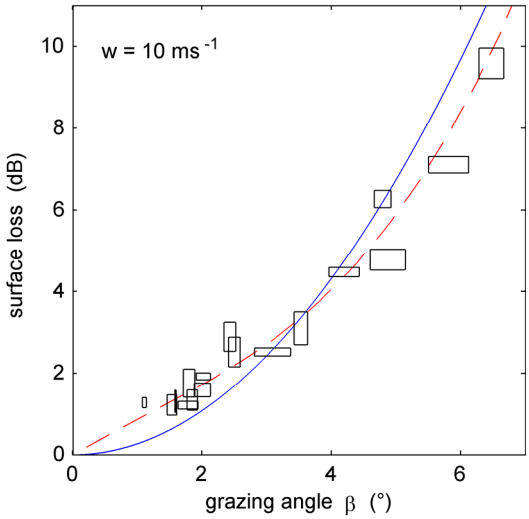

Figure 4. Reflection Loss per bounce: blue - KA, red dashed - SSA, boxes - stochastic; 10 m/s wind speed $w_{19.5}$, 3200 Hz

Coherent and Incoherent Reflection Loss

The RAMSurf model was used to compute the coherent pressure field referenced to the pressure one metre from the source, across a grid in range r and depth z. One run was executed for each of $k \in \{1, \cdots, n\}$ realisations of the rough surface. Denoting the coherent pressure p_k at grid point (r, z), using complex arithmetic we have $p_k = x_k + iy_k$ for the kth surface realisation. The arithmetic mean $\overline{p_c}$ of the complex pressure values was determined as

$$\overline{p_c} = \frac{1}{n}\sum_{k=1}^{n} x_k + i\frac{1}{n}\sum_{k=1}^{n} y_k \qquad (5)$$

and represents the coherent average, across all surface realisations, of the pressure values at (r, z). In a practical sense, it accounts for the average effect of the reflection from a rough surface, across equivalent but independent surface bounces, when the received signal is processed as coherent pressure, as is typical with processing returns from linear FM sonar pulses. Transmission Loss (TL), as a positive quantity, for the averaged coherent field is $TL_c = -20\log_{10}\left|\overline{p_c}\right|$.

Taking $p_u = x_u + iy_u$ as the coherent pressure at (r, z) when there is an unperturbed sea surface, the corresponding TL is $TL_u = -20\log_{10}\left|\overline{p_u}\right|$. In general, a metric for the component of loss due to surface reflection loss is then

$$\Delta TL_c = TL_c - TL_u \,. \tag{6}$$

An alternative expression of loss may be based on the incoherent average of the pressure values p_k as

$$p_i = \left[\frac{1}{n} \sum_{k=1}^{n} \left({x_k}^2 + {y_k}^2 \right) \right]^{1/2}, \tag{7}$$

leading to the metric for reflection loss as

$$\Delta TL_i = TL_i - TL_u \,, \tag{8}$$

where $TL_i = -20 \log_{10} p_i$. Use of the incoherent, or energy, average is relevant to processing returns from CW pulses, as these are commonly processed by a square-law detector (e.g. page 385 Urick 1983), for which output is proportional to the square of sound pressure input. Also, a diffuse component may be defined as $\left({p_i}^2 - \left| \overline{p_c} \right|^2 \right)^{1/2}$.

Figures 5 and 6 show *TL* based on averaged received signal levels, across range and depth points, for a test scenario with an omnidirectional source at 18 m depth, with a 64 m isothermal surface duct overlying an isovelocity ocean of infinite extent. Here, the RAMSurf model has been run for a large number (40) of random replications of a sea surface displaced vertically such that the PM wave spectrum was satisfied. Each RAMSurf run simulated a bottomless ocean through the inclusion of a highly absorbent region at depths 200 m and greater. The data in the figures has been averaged coherently for Figure 5 and incoherently for Figure 6. This scenario (3200 Hz for 10 m/s wind speed) causes a high *TL*. Note that the refractive effects of the wind-induced bubbles have been included through the incorporation of the changes to the sound speed profile discussed in the following section, and shown in Figure 7. As is evident from these figures, the coherent average of the received signal values shows a greater loss relative to the incoherent averaging.

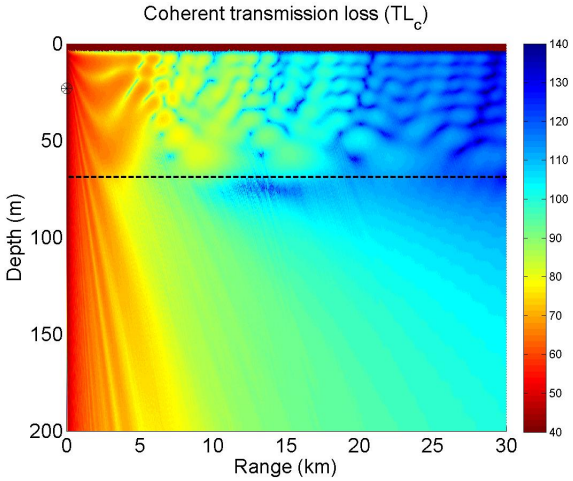

Figure 5. Transmission Loss TL_c for averaged coherent field, source at 18 m, 10 m/s wind speed $w_{19.5}$, 3200 Hz

As RAMSurf must be run with every field point being at zero or greater depth, for these simulations the field has been displaced downward by 5 m. Thus the bottom of the surface duct, shown by the dashed line, and the position of the source, shown by a symbol in each figure, are each displaced in this way. The reverse of this displacement was made before comparisons were achieved with the field for the unperturbed surface. Of interest is that the energy scattered from the surface reflections may be seen in these figures.

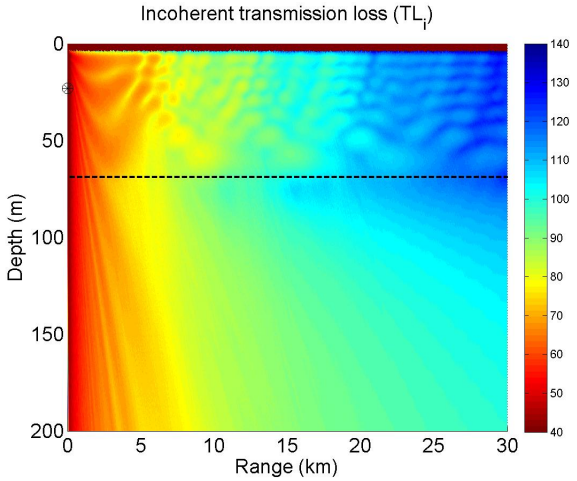

Figure 6. Transmission Loss TL_i for averaged incoherent field, source at 18 m, 10 m/s wind speed $w_{19.5}$, 3200 Hz

INCLUSION OF REFRACTION DUE TO WIND-INDUCED BUBBLES

Ainslie's (2005, 2010) simulations of surface reflection loss involved the incorporation of the Hall-Novarini model of bubble population as a function of depth and wind speed. The presence of bubbles reduces the sound speed through an increase in the compressibility of the bubbly water versus bubble-free water. The result is a departure of the sound speed versus depth function from that appropriate to an isothermal mixed layer. Figure 7 shows this variation near the ocean surface for a range of wind speeds. It is evident that the effect is confined to the top few metres of the ocean, and that the resultant sound speed gradients are very large, being of the order 10 s^{-1}, in comparison to the isothermal gradient of 0.017 s^{-1} from the depth (pressure) effect. The effect of the bubbles on sound speed extends, in depth, to just several acoustic wavelengths, at most, for frequencies of interest.

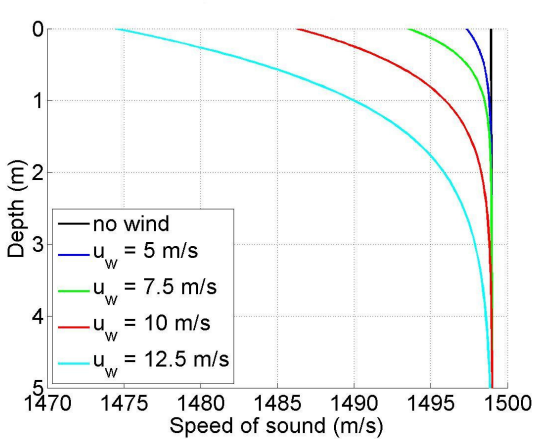

Figure 7. Sound speed near surface, with bubble effects, wind speeds $w_{19.5}$ 5, 7.5, 10, 12.5 m/s, after Ainslie (2005)

Typically, for an isothermal surface duct, the change in sound speed at the ocean surface due to wind-induced bubbles ex-

ceeds the 0.017*D* m/s sound speed variation that exists over the entire duct depth *D* due to the depth effect. For a 64 m duct, the latter results in a 1.09 m/s sound speed difference across the duct depth, whereas the effect from bubbles is much greater, as shown by the data in Figure 7. If refraction follows Snell's Law, the grazing angle at the ocean surface, for sound travelling in an isothermal surface duct with a region of wind-induced bubbles, will be almost completely determined by the bubble phenomena. Based on the resultant surface sound speed, the angle of incidence at the surface for all surface-ducted energy is $\beta_1 \approx 0.0042(w_{19.5})^{3/2}$ radians, for wind speed of the order of 5 m/s or more. Although it is beyond consideration in the present paper, it may be stated that the wind-induced sound speed reductions near the ocean surface will cause the formation of a mini-duct within the mixed layer duct. Simplification of the models of roughness loss described by Equations (2) and (4) become feasible by substituting for surface grazing angle β_1 with the above expression. This results in the following expressions for the KA model and the linear approximation to the SSA:

For KA model

$$RL \approx 1.5\times10^{-13} f^2 (w_{19.5})^7 \text{ dB.} \quad (9)$$

For linear approximation to SSA model

$$RL \approx 1.16\times10^{-9} f^{3/2} (w_{19.5})^{9/2} \text{ dB.} \quad (10)$$

For a particular situation, the larger value from these two expressions would be used, as explained earlier for the case of Equations (2) and (4). The results from Equation (10), for wind speed $w_{19.5}$ = 10.6 m/s (same as w_{10} = 10 m/s), are similar to those in Ainslie's fig. 8.2 (2010), as the analyses are similar. For some frequencies, however, the loss value from Equation (9) exceeds that from Equation (10), indicative of the increase of the KA model (and SSA model) away from the linear approximation to the SSA model for relevant angles of surface incidence. The simplifications of Equations (9) and (10) are, of course, based on the ray approximation to transmission through the bubble zone and so are contingent upon the refraction in that zone occurring in accord with Snell's law.

Adherence to WKBJ Approximation

Ray models are based on a number of assumptions, and are, at best, convenient approximations to a more complete solution of the wave equation. As is well known, a plane wave ray solution is limited in the shallowness of the angle at which sound may impinge upon a zone of high sound speed gradient. Here, the Wentzel-Kramers-Brillouin-Jeffreys (WKBJ) approximation must be satisfied. This may be shown to require (e.g. Frisk (1994) equation 7.27)

$$\frac{1}{4\left[k_x(z)^2\right]}\left|\frac{d^2}{dz^2}\left[\ln\left[k_x(z)^2\right]\right]-\left\{\frac{d}{dz}\left[\ln\left[k_x(z)\right]\right]\right\}^2\right| << 1 \quad (11)$$

where $k_x(z) = [\omega/c_w(z)]\sin\beta(z)$ and z is depth. Figure 8 illustrates the zones of range and depth, in red, for which the approximation is not valid at 3200 Hz for the test scenario with a source at 18 m depth in a 64 m isothermal duct, for which the bubble-caused sound speed variations appropriate to 7.5 m/s wind are included. In approximating the requirement for the left-hand side of expression (11) to be <<1, failure was judged to occur when it exceeded 0.05. For clarity, Figure 8 shows the rays to the first surface bounce, only.

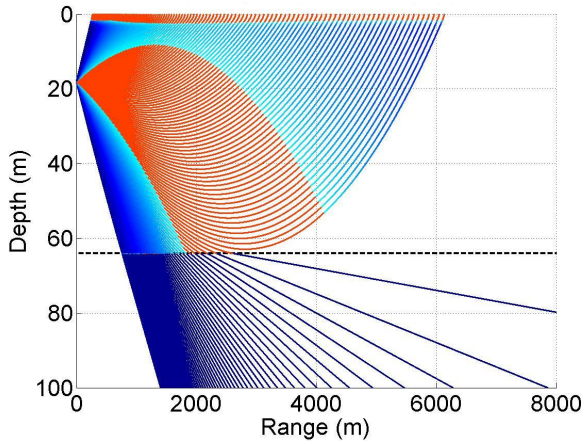

Figure 8. Adherence to WKBJ approximation for ray calculation, 7.5 m/s wind speed $w_{19.5}$, 3200 Hz

Clearly, ray modelling and Snell's Law may fail in the region near the surface in which the wind-induced bubbles are located. It may be noted that the WKBJ approximation also fails near ray turning points, as is well known (e.g. Frisk (1994)). Although not shown here, calculations similar to that in Figure 8 show that the extent of the violation of the WKBJ approximation is reduced for higher frequencies.

Wave Model of Refraction

In order to better describe refraction phenomena in the bubbly zone, a wave-based solution was obtained for the angle of incidence at the ocean surface as a function of the angle of incidence at the bottom of the bubbly zone. This was based on Brekhovskikh's analysis (1960) for plane waves in layered-inhomogeneous media. Ainslie (2005) achieved an alternative wave description, however, that relied upon numerical simulation not suited to convenient calculation. The essence of the problem is that, in the region of strong SSP gradient, the direction of the phase velocity follows Snell's Law, whilst the direction of the intensity vector, does not.

One of Brekhovskikh's example cases (the transitional layer) contained a sound speed variation with depth which closely resembled that implied by Ainslie's use of the Hall-Novarini model of bubble population. From use of Brekhovskikh's analysis, through techniques not detailed in this paper, the desired solution to the surface incidence of the intensity vector was then found. Figure 9 shows the closeness of the sound speed variation achieved using Brekhovskikh's "transitional" scenario to that obtained from Ainslie's analysis (2005) for the case of a wind speed at 19.5 m above the surface of 7.5 m/s.

Examples of the derived functions of grazing angle of the intensity vector at the ocean surface, based on this approach, are shown in Figures 10 to 13. Each figure shows a curve (the solid line) giving the Snell's Law result, for which the angle of incidence of at the surface β_1 is related to the angle of incidence at the bottom of the bubble zone β_2 by the well known expression $\cos\beta_1/c_{w_1} = \cos\beta_2/c_{w_2}$ (e.g. Lurton (2002) page 42). Each figure also shows, as a dashed line,

the result from the application of Brekhovskikh's analysis as mentioned above. In the examples in Figures 10 and 12, the "Brekhovskikh" result gives a relatively small difference between angles β_2 and β_1. That is, for these cases (3200 Hz for 7.5 m/s wind, 6000 Hz for 5 m/s wind) there is little refraction of the intensity vector in the bubbly zone. For higher wind speeds, however, the situation is changed. Figure 11 shows that with 12.5 m/s wind, at 3200 Hz the surface grazing angle of the intensity vector is greatly different to that below the bubbly region. Similarly, Figure 13 shows that a wind speed of 7.5 m/s gives rise to greatly increased refraction of the intensity vector at 6000 Hz.

Now, from ray acoustics, for an isothermal duct, $\beta_1 = \sqrt{2 d_h \, g / c_w}$, where d_h is the depth at which a ray is launched in a horizontal direction, and g is sound speed gradient. Hence, for a source at 18 m depth in a 64 m duct for the test scenario, surface angles of incidence in bubble-free water will be confined to between 1.2° and 2.2°, the latter corresponding with a limiting ray. Clearly, these angles will be nearly the same as incident angles β_2 below the bubbly zone in the with-bubbles case. As the "Snell's Law" and "Brekhovskikh" curves in Figure 13 are not greatly different for this span of angles incident below the bubbly zone, this indicates that the wave solution has a similar effect to the ray (Snell's Law) result for 7.5 m/s wind at 6000 Hz.

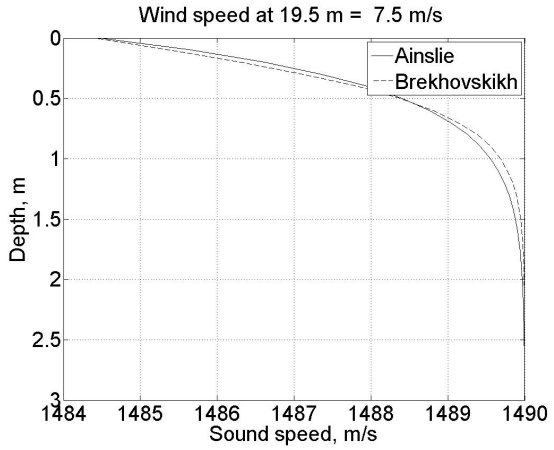

Figure 9. Sound speed variation in bubbly region (i) after Ainslie (2005), (ii) modelled with Brekhovskikh's "transitional" scenario, 7.5 m/s wind speed

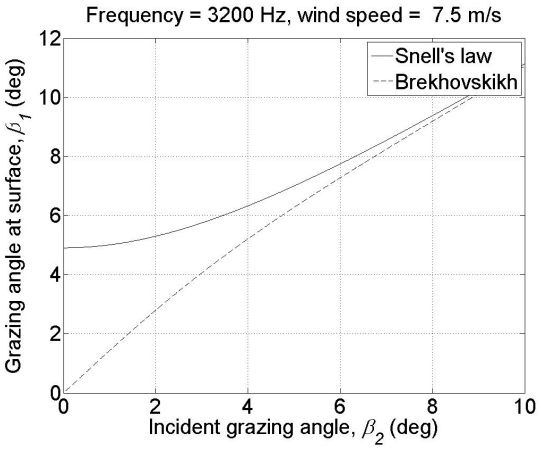

Figure 10. Grazing angle of intensity vector at surface vs incidence angle at bottom of bubbly region, 7.5 m/s wind speed, 3200 Hz

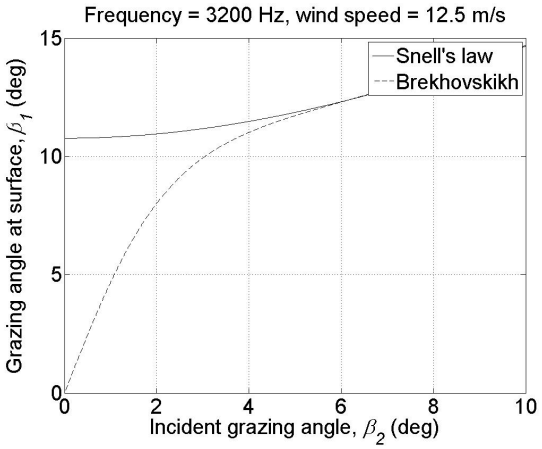

Figure 11. Grazing angle of intensity vector at surface vs incidence angle at bottom of bubbly region, 12.5 m/s wind speed, 3200 Hz

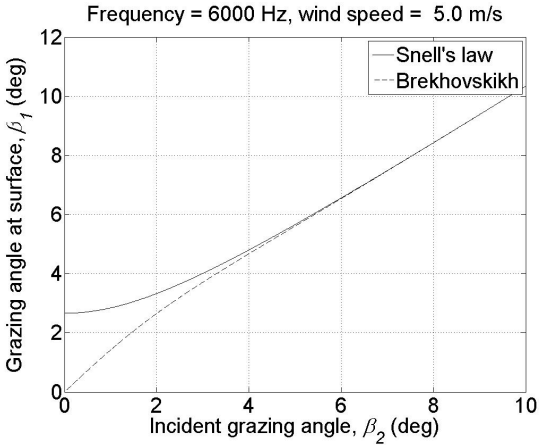

Figure 12. Grazing angle of intensity vector at surface vs incidence angle at bottom of bubbly region, 5 m/s wind speed, 6000 Hz

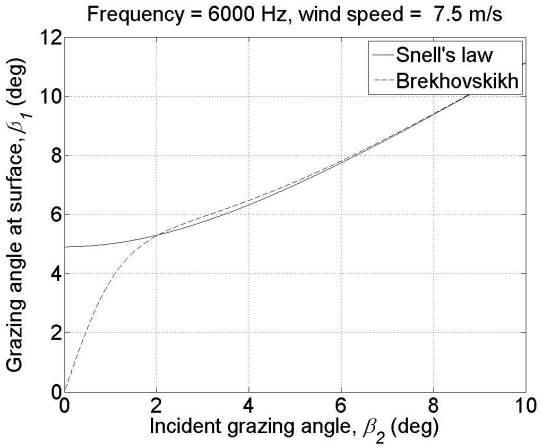

Figure 13. Grazing angle of intensity vector at surface vs incidence angle at bottom of bubbly region, 7.5 m/s wind speed, 6000 Hz

STOCHASTIC MODELLING OF DUCTED TRANSMISSION

Acoustic transmission for a surface ducted scenario was modelled, using the stochastic modelling regime outlined earlier. In this way the field was computed, first for a smooth surface, then with the surface described as rough, with 40 random replications of the rough sea surface. The averaged

coherent field was determined from the rough surface runs. The ocean scenario was the same as that used previously by the authors (Jones et al., 2010): isothermal surface duct over an infinitely deep isovelocity ocean; duct depth 64 m; source depth 18 m; frequency 3200 Hz. Wind speed $w_{19.5}$ was set to 7.5 m/s, and the resultant variation in sound speed due to wind-induced bubbles was based on the Hall-Novarini bubble population model, as mentioned earlier (see Figure 7).

Figure 14 shows the component of *TL*, ΔTL , due to surface reflection loss, computed for the test scenario by: (i) the ray model Bellhop incorporating the SSA model of *RL*; (ii) the stochastic modelling method based on averaged received coherent pressure. In each case the sound speed profile explicitly included the effect of isothermal water plus wind-induced bubbles for wind speed $w_{19.5}$ of 7.5 m/s. The values of ΔTL were obtained by subtracting the corresponding rough surface *TL* data from the *TL* data for a smooth surface in the case of the RAMSurf modelling, and from the *TL* data when surface loss was set at zero for the Bellhop modelling. For this work, Bellhop was run in phase coherent mode.

The value ΔTL based on ray modelling is clearly much greater than that from the stochastic modelling. This may be understood by reference to the angles of incidence expected at the surface by (i) ray modelling, (ii) wave modelling. From Figure 10, making the earlier-mentioned assumption that a limiting ray (or wave) will be incident on the bottom of the bubbly zone at 2.2°, Snell's Law and ray modelling will describe the grazing angle at the surface as about 5.3°, whereas for full wave modelling a grazing angle of the intensity vector of about 2.8° is expected. Each modelling approach incorporates reflection loss as described by the SSA model: the ray model incorporates it explicitly, and the RAMSurf stochastic modelling does so implicitly by virtue of the stochastic modelling matching the SSA loss values, e.g. Figure 4. Hence, loss values per bounce may be expected as shown in Figure 1, notwithstanding the slight difference in frequency (3000 Hz vs 3200 Hz). Loss per bounce values of about 2.2 dB (5.3° incidence from ray modelling) and 1.0 dB (2.8° incidence from RAMSurf modelling) are expected. Assuming 5 surface bounces to 30 km range for the limiting ray, the total expected values of surface loss are very close to those values of ΔTL shown in Figure 14. Significantly, the results for the RAMSurf modelling are consistent with that expected based on the wave nature of refraction described earlier, and as shown in Figure 10.

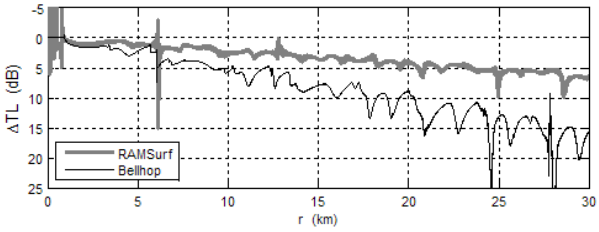

Figure 14. *TL* component due to Reflection Loss; 7.5 m/s wind speed $w_{19.5}$, 3200 Hz, test scenario

This modelling was repeated for the same wind speed and frequency combination, using a different implementation of RAMSurf, and using a different Gaussian beam ray model, so that the results in Figure 14 might be confirmed. Here, RAMSurf was used with a different spatial sampling regime, and the alternate ray model was run in phase-incoherent mode. The result from this repeat modelling, shown in Figure 15, is very close in its replication of that shown in Figure 14 thus giving confidence in the modelling approaches, and in the wave model of refraction. The 2nd of these modelling approaches was used for the additional work described below.

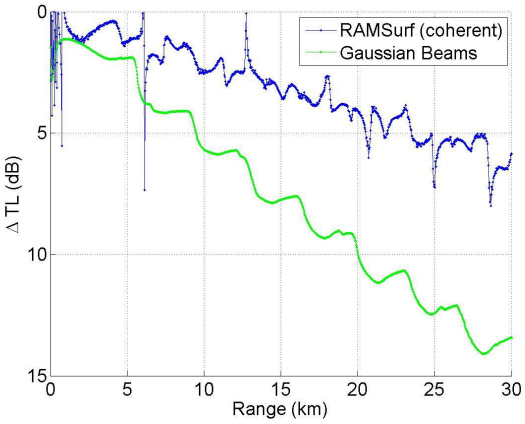

Figure 15 *TL* component due to Reflection Loss; 7.5 m/s wind speed $w_{19.5}$, 3200 Hz, test scenario

Additional examples of calculation of the component of *TL*, ΔTL , due to surface reflection loss, were made for other wind speed/frequency cases for which the result might be anticipated. Firstly, RAMSurf and Gaussian beam ray model calculations were carried out for wind speed $w_{19.5}$ of 5 m/s and frequency 6000 Hz. From the expectations of refraction in the bubbly zone shown in Figure 12 for the limiting ray incident below the bubbly zone at 2.2°, the ray model will describe a surface arrival at about 3.4°, whereas RAMSurf modelling is expected to describe the wave-model result at about 2.8°. From Figure 2, surface loss values expected per bounce are about 1.1 dB and 0.8 dB, respectively. Bearing in mind that the limiting ray exhibits 5 surface bounces to 30 km, the ΔTL values shown in Figure 16 are well matched to expectations.

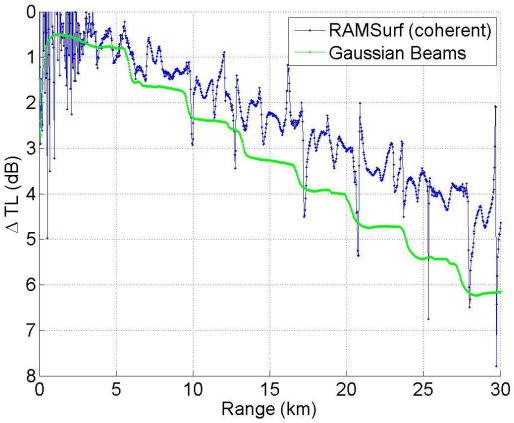

Figure 16 *TL* component due to Reflection Loss; 5 m/s wind speed $w_{19.5}$, 6000 Hz, test scenario

A further example calculation of the components of *TL*, ΔTL , due to surface reflection loss, is shown in Figure 17 for wind speed $w_{19.5}$ of 7.5 m/s and frequency 6000 Hz. In this case, from Figure 13 for the limiting ray incident below the bubbly zone at 2.2°, both the ray model and RAMSurf modelling are expected to describe a surface arrival at about 5.3°. From Figure 3 surface loss values expected per bounce are about 7 dB for each modelling approach. Bearing in

mind that the limiting ray exhibits 5 surface bounces to 30 km, the ΔTL values shown in Figure 17 are consistent with expectations. Note that the ΔTL value from the Gaussian beam ray model reaches a limit at about range 15 km. It is believed that this is an artefact of the model for scenarios with high transmission loss.

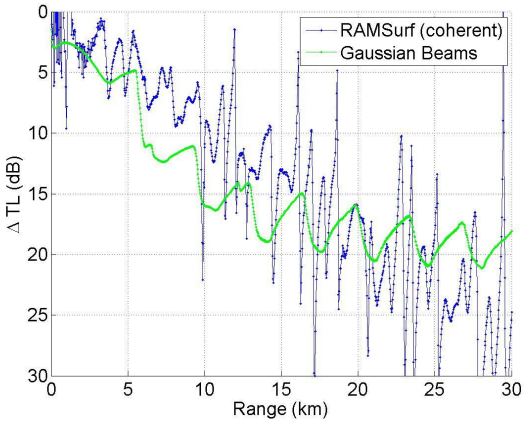

Figure 17. *TL* component due to Reflection Loss; 7.5 m/s wind speed $w_{19.5}$, 6000 Hz, test scenario

DISCUSSION

The modelling of the wave nature of refraction, using Brekhovskikh's analysis (1960) for plane waves in layered-inhomogeneous media, for which all aspects and results are not shown in this paper, has revealed those combinations of wind speed and frequency for which the refractive effects of wind-induced bubbles are negligible. Using the model of wind-induced bubbles published by Ainslie (2005), for wind speed 5 m/s the effect of bubbles is negligible for frequencies 3 kHz and less; for wind speed 7.5 m/s it is negligible for frequencies 2 kHz and less; for wind speed 10 m/s it is negligible for frequencies 1 kHz and less. In these situations, surface loss per bounce may be modelled using either the full SSA result or the greater of Equations (2) and (4). Conversely, there are combinations of wind speed and frequency for which the refractive effects of wind-induced bubbles may be adequately described by Snell's Law and ray modelling, and loss values per bounce may be obtained from the greater of Equations (9) and (10). For wind speed 5 m/s this is the case for frequencies 10 kHz and more; for wind speed 7.5 m/s it is for frequencies 6 kHz and more; for wind speed 10 m/s it is for frequencies 3 kHz and more. For intermediate combinations of wind speed and frequency, the wave nature of refraction in the bubbly zone must be modelled. This is, however, feasible using an approach similar to that used for this paper, and it is quite conceivable that such a calculation of sea surface incidence angle may be incorporated within a conventional ray model of transmission. Once the grazing angle of the intensity vector at the surface is known, the loss per bounce follows from the greater of Equations (2) and (4). In this way, a physics-based model of surface reflection loss is achievable within an existing ray model.

CONCLUSIONS

Stochastic modelling of the component of Transmission Loss due to sea surface roughness appears to confirm the expectations from the application of the small slope model of coherent surface loss used by Williams et al. (SSA). This model, in turn, may be readily approximated by simple algorithms. The refractive effects of wind-induced bubbles have, however, potential to cause significant difficulty to the way in which this modelling of sea surface reflection loss may be included in conventional ray models, but a solution is now within reach. Based on the modelling of the wave effects of refraction within the zone near the surface in which wind-induced bubbles exist, it appears that for some low combinations of wind speed and frequency the bubble effects are negligible, whereas for other higher combinations the refraction in the near-surface region may be described simply by Snell's law, combined with the refraction expected with the bubble model which is employed. The bubble model adopted for this work is that which has been used by Ainslie. For intermediate combinations of wind speed and frequency, the result from a wave-based model of refraction in the bubble zone may be used to describe the incidence at the surface, and a loss value may be determined by application of the SSA model or its simplified alternative. In this way, a physics-based model of surface reflection loss is expected to be achievable within existing ray models.

REFERENCES

Ainslie, M.A. 2005, 'Effect of wind-generated bubbles on fixed range acoustic attenuation in shallow water at 1 – 4 kHz', *J. Acoust. Soc. Am.*, vol. 118, pp 3513 – 3523

Ainslie, M.A. 2010, *Principles of Sonar Performance Modeling*, Springer-Praxis.

Brekhovskikh, L.M. 1960, *Waves in Layered Media*, Academic Press

Brekhovskikh, L.M. and Lysanov, Yu.P. 2003, *Fundamentals of Acoustics*, 3rd edition, Springer-Verlag, New York

Frisk, G.V. 1994, *Ocean and Seabed Acoustics*, PTR Prentice-Hall, New Jersey

Jones, A.D., Duncan, A.J., Maggi, A., Clarke, P.A. and Sendt, J. 2010, 'Aspects of practical models of acoustic reflection loss at the ocean surface', *Proceedings of 20th International Congress on Acoustics, ICA 2010*, Sydney, Australia

Jones, A.D., Duncan, A.J., Bartel, D.W., Zinoviev, A. and Maggi., A. 2011 'Sonar Reflection Loss at the Ocean Surface for Small Grazing Angles', *Proceedings of 4th International Conference and Exhibition on Underwater Acoustic Measurements: Technologies & Results*, Kos, Greece, pp 479 - 484

Lurton, X. 2002, *An Introduction to Underwater Acoustics,* Praxis Publishing Ltd.

Marsh, H.W., Schulkin, M. and Kneale, S.G. 1961, 'Scattering of Underwater Sound by the Sea Surface', *J. Acoust. Soc. Am.*, vol. 33, pp 334 – 340

Medwin, H. and Clay, C.S. 1998, *Fundamentals of Acoustical Oceanography*, Academic Press

NRL n.d., <ftp://ftp.ccs.nrl.navy.mil/pub/ram/RAM/>

Ogilvy, J.A. 1987, 'Wave scattering from rough surfaces', *Rep. Prog. Phys.* Vol. 50, pp 1553 – 1608

Tolstoy, I. and Clay, C.S. 1987, *Ocean Acoustics: Theory and Experiment in Underwater Sound*, American Institute of Physics, New York

Urick, R.J. 1983, *Principles of Underwater Sound*, 3rd edition, Peninsula Publishing, Los Altos

Wagner, R.J. 1967, 'Shadowing of Randomly Rough Surfaces', *J. Acoust. Soc. Am.*, vol. 41, no. 1, pp 138 – 147

Williams, K.L., Thorsos, E.I. and Elam, W.T. 2004, 'Examination of coherent surface reflection coefficient (CSRC) approximations in shallow water propagation', *J. Acoust. Soc. Am.*, vol. 116, no. 4, pp 1975 – 1984